Journal of the Korean Society of Marine Environment & Safety
Research Paper
Vol. 27, No. 3, pp. 409-420, May 31, 2021, ISSN 1229-3431(Print) / ISSN 2287-3341(Online) https://doi.org/10.7837/kosomes.2021.27.3.409

Reduction of UKC for Very Large Tanker and Container Ship in Shallow Water

Sang-Min Lee*†

* Professor, Division of Marine Industry Transportation Science and Technology, Kunsan National University, Kunsan, 54150, Republic of Korea

Abstract : *The decrease in under keel clearance (UKC) due to the increase of draft that occurs during advancing and turning of very large vessels of different types was analyzed based on computational fluid dynamics (CFD). The trim change in the Duisburg test case (DTC) container ship was much smaller than that of the KRISO very large crude oil carrier 2 (KVLCC2). The sinkage of both ships increased gradually as the water depth became shallower. The amount of sinkage change in DTC was greater than that in KVLCC2. The maximum heel angle was much larger for DTC than for KVLCC2. Both ships showed outward heel angles up to medium-deep water. However, when the water depth became shallow, an inward heel was generated by the shallow water effect. The inward heel increased rapidly in very shallow water. For DTC, the reduction ratio was very large at very shallow water. DTC appeared to be larger than KVLCC2 in terms of the decreased UKC because of shallow water in advancing and turning. In this study, a new result was derived showing that a ship turning in a steady state due to the influence of shallow water can incline inward, which is the turning direction.*

Key Words : *UKC, KVLCC2, DTC, CFD, Sinkage, Trim*

1. Introduction

Based on the economy of scale and energy efficiency, 24,000 twenty-foot equivalent unit (TEU)-class ultra-large container ships have been built recently and are being used for actual cargo transportation. When very large crude oil carriers (VLCCs) and super-large container ships navigate in shallow waters, such as straits, canals, and coastal areas, it can lead to potential maritime accidents, such as ships running aground. Therefore, it is necessary to accurately identify and manage the reduced clearance depth caused by the change in the vertical movement of the vessel as it navigates in shallow water.

As the size of ships has increased, their breadth has tended to increase compared to their length. If the breadth increases this way, there is a high risk that the ship's bilge could touch the sea floor when the ship inclines in shallow water. An outward or inward heel occurs when the ship turns. Thus, it is necessary to study the correlation between the ship's heel generation and clearance depth.

As vessels navigate in shallow water, they show increased resistance and decreased under keel clearance (UKC) due to squat. Squat consists of sinkage and trim, and means a reduction of UKC. When the water depth is lower, the flow field around the hull changes and the hydrodynamic force that is applied to the ship fluctuates, which results in a phenomenon that is different from the ship's maneuverability and propulsion performance at deeper depths.

Relating to the increased resistance, the characteristics of viscous and wave resistance caused by the shallow water and scale effects were analyzed (Zeng et al., 2019; Zeng et al., 2020). Research on the maneuvering performance of ships in shallow water is also underway. By utilizing experiments to analyze maneuverability in shallow water, Xu et al. (2020) reported that the turning circle increased, and the course stability decreased. Tang et al. (2020) demonstrated that the shallower the water depth, the stronger its effect on maneuverability reduction. Lee and Hong (2017) conducted a study to compare the course stability index of very large ships by obtaining the hydrodynamic derivatives in shallow water using computational fluid dynamics (CFD).

In a theoretical study related to the squat of ships in shallow water, Kijima et al. (2002) researched a method for estimating a ship's sinkage and trim by using a simple empirical formula. Gourlay (2008) employed the slender-body theory to calculate ship sinkage in various waterways. Alderf et al. (2011) used the finite element method to describe how the shape of the seabed affects the dynamic sinking of ships.

To estimate the squat in shallow water, studies have recently targeted various conditions by using existing empirical formulas as well as CFD. Tezdogan et al. (2016) analyzed the squat and resistance characteristics of ships for various depth Froude numbers

† smlee@kunsan.ac.kr, 063-469-1814

(*Frh*) using Duisburg test case (DTC) container ship. Terziev et al. (2018) conducted a study that compared and analyzed sinkage, trim, and resistance in various types of channels. Bechthold and Kastens (2020) studied squat estimation in extremely shallow water for three post-Panamax container ships.

Studies have analyzed the phenomena of squat changes in shallow water by conducting extensive water tank experiments on Kriso container ship (KCS) and Kriso very large crude oil carrier 2 (KVLCC2) model ships (Yun et al., 2014a; Yun et al., 2014b). An experimental squat analysis was performed by considering the width of the canal (Lataire et al., 2012). Verwilligen et al. (2019) measured the vertical motions in nine ultra-large container ships and extensively studied the correlation between various environmental factors and squat.

Until now, although studies on the increase in draft caused by the sinkage and trim of ships advancing in shallow water have been conducted, the characteristics of reducing UKC by estimating the increased draft caused by the heeling of a turning ship have not been analyzed. Additionally, studies have been conducted only on the same ship type as the analysis target, and few cases have been reported where ships of different shapes were compared with each other.

This study calculates the longitudinal squat based on CFD by using the amount of change in the trim angle and sinkage caused by the vertical movement of the advancing ships. In addition, the heel angle caused by the roll moment acting on the turning vessel was determined, and the lateral squat value was calculated based on this list effect to analyze the reduced UKC. The simulation was carried out for the actual sizes of the KVLCC2 tanker ship and DTC container ship, according to different water depths.

2. Numerical analysis

2.1. Computational method

In this study, STAR-CCM+, a commercial CFD program based on the finite volume method was used for numerical simulations. The Reynolds-averaged Navier-Stokes (RANS) equations for incompressible flows without body forces are denoted as tensor notations in Cartesian coordinates, as follows (Ferziger and Peric, 2002):

$$\frac{\partial(\overline{\rho u_i})}{\partial x_i} = 0 \tag{1}$$

$$\frac{\partial(\overline{\rho u_i})}{\partial t} + \frac{\partial}{\partial x_j}(\overline{\rho u_i}\,\overline{u_j} + \overline{\rho u'_i u'_j}) = -\frac{\partial \bar{p}}{\partial x_i} + \frac{\partial \bar{\tau}_{ij}}{\partial x_j} \tag{2}$$

in which $\bar{\tau}_{ij}$ represents the mean viscous stress tensor components:

$$\bar{\tau}_{ij} = \mu\left(\frac{\partial \bar{u}_i}{\partial x_j} + \frac{\partial \bar{u}_j}{\partial x_i}\right) \tag{3}$$

where ρ is the density, $\bar{u}_i$ denotes the averaged Cartesian components of the velocity vector, $\overline{\rho u'_i u'_j}$ denotes the Reynolds stresses, and μ is the dynamic viscosity.

The temporal discretization of the unsteady term used a first-order temporal scheme, and a second-order scheme was applied to discretize convection terms. The SIMPLE method was used for velocity-pressure coupling. The realizable $k-\epsilon$ model was utilized in the turbulence model and all y+ wall treatment was applied.

The free surface was analyzed by applying the volume of fluid (VOF) method, and the range of $\Delta t = 0.00225 - 0.0045 L/V_S$ was selected for numerical calculations.

The motion of the hull was calculated by applying the dynamic fluid-body interaction technique provided by STAR-CCM+.

2.2. Computational conditions

Table 1 shows the main specifications of full-scale KVLCC2 and DTC for simulating the squat characteristics. The numerical simulation conditions included a ship speed of 7 knots (*Fr*=0.064) for KVLCC2 and 13 knots (*Fr*=0.113) for DTC, considering navigation in shallow water.

Table 1. Main particulars of KVLCC2 and DTC

	KVLCC2	DTC
Lpp (m)	320.0	355.0
B (m)	58.0	51.0
T (m)	20.8	14.5
Δ (m^3)	312,622.0	173,467.0
C_B	0.8098	0.6610
KG (m)	18.60	23.28
GM (m)	5.71	1.68
V_S (kt)	7.0	13.0
Fr	0.064	0.113
Re	1.147×10^9	2.364×10^9

Fig. 1 shows the computational domain used in this study, a Cartesian coordinate system was used where the +x, +y and +z axes represent the forward, the port direction of the ship, and the opposite direction of gravity, respectively.

The calculation area is 1.5*L* to the fore body, 2.5*L* to the aft

body, and 2*L* away laterally. From the water's surface, the top is 3*T* away. The distance from the free surface to the seabed is 5.0, 2.0, 1.5, and 1.2*T*, *L* and *T* denote the length between perpendiculars and the draft, respectively.

H/T>3.0 refers to deep water, 1.5<*H/T*<3.0 refers to medium-deep water, 1.2<*H/T*<1.5 refers to shallow water, and *H/T*<1.2 refers to very shallow water, according to PIANC (1992). The differences between the ranges of deep and shallow water were defined based on these measurements: *H/T*=5.0 was applied to deep water, *H/T*=2.0 to medium-deep water, *H/T*=1.5 to shallow water, and *H/T*=1.2 to very shallow water, where *H* denotes the depth of the water.

The inlet, top, and side boundaries were selected as the velocity inlets. The hull surface and bottom boundary were designated as being in a no-slip boundary condition. Numerical computations were performed using the VOF wave damping functionality of the software, with a damping length of 1.0*L* to avoid waves reflecting into the domain.

Spatial and hull-surface meshes were generated using a trimmed mesh and prism layer, respectively. To implement the flow simulation in the head, stern, free surface, and divergent regions more precisely, the grid was created to be denser than the base size by using volumetric control.

The mean y+ values of full-scale KVLCC2 and DTC at *H/T*=1.2 are 266 and 478, respectively, where y+ is the dimensionless wall distance. The detailed grid convergence uncertainty is described in Section 3.1.

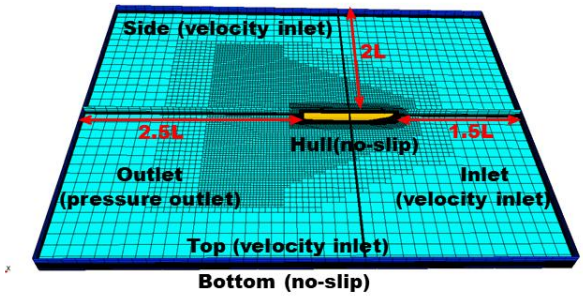

Fig. 1. Computational domain, grid distribution and boundary condition.

Table 2. UKC and *Frh* for KVLCC2 and DTC

		H/T=5.0	H/T=2.0	H/T=1.5	H/T=1.2
KVLCC2	UKC (m)	83.20	20.80	10.40	4.16
	Frh	0.113	0.178	0.206	0.230
DTC	UKC (m)	58.00	14.50	7.25	2.90
	Frh	0.251	0.397	0.458	0.512

Table 2 shows the UKC and *Frh* of each vessel according to the water depth. As shown in Table 2, simulations were carried out in each of the four types of water depth. The water depth did not change during the simulation.

In this study, the influence of oceanographic conditions and wave response was not considered while estimating the amount of UKC changes.

Fig. 2 depicts the static UKC (SUKC) and draft *T* in the stationary state. Additionally, it shows the increased draft (ΔT) due to the sinkage and trim generated as the ship moves, dynamic UKC (DUKC), and changed draft *T'*.

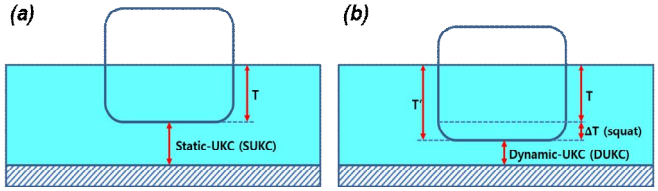

Fig. 2. Definition of (a) static UKC (SUKC) and (b) dynamic UKC (DUKC).

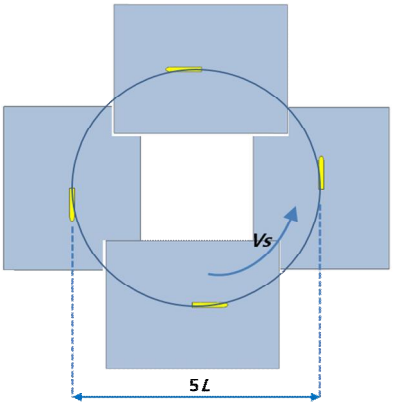

Fig. 3. Turning simulation to compute lateral squat.

The UKC reduction was calculated by separating it into two fields. The first field was used to calculate the squat of the ship advancing at a speed V_S in the longitudinal direction, and the numerical computation was performed in the free mode, with only the vertical motion heave and pitch. The second field was used to obtain the squat (lateral squat) of the vessel during turning. The lateral squat was estimated by conducting a simulation considering only the roll motion. The longitudinal squat is based on the amount of draft increase obtained from the displacement of the center of gravity due to the heave and pitch motions, and the lateral squat is calculated using the amount of draft increase obtained from the maximum inclination angle due to the roll

motion. In the simulation to calculate the longitudinal squat, the computational domain does not move and the fluid corresponding to the speed of the ship enters the inlet. The simulation for obtaining the lateral squat is performed by assuming that the computational domain and the ship are rotating together at a distance of 2.5*L* from the center of turning as shown in Fig. 3.

3. Computation results and discussion

3.1. Mesh sensitivity and verification analysis

To validate the numerical method, the vessel's resistance and sinkage were compared with the experimental data (EFD). The experimental data and numerical results were compared for both types of vessels at *H/T*=1.2 using KVLCC2 1/45.714 and DTC 1/89.11 scale models. In the absence of experimental data (sinkage of KVLCC2), the result of the present study and that of another CFD were compared with each other.

The total resistance *Rt* and sinkage are shown in Table 3, along with the experimental and calculated values for each vessel. When compared with the experimental data, the errors of the sinkage calculation results appear larger than those of the resistance. This trend was also discussed in the study by Yuan et al. (2019). It is assessed that the reason for this phenomenon is that the value of the sinkage is too small. It seems that the data of the tank experiment and the present calculation results are relatively consistent.

Table 3. Validation test for DTC and KVLCC2 with resistance and sinkage at *H/T*=1.2

	KVLCC2 (1/45.714 scale)		DTC (1/89.11 scale)	
	Rt (N)	sinkage (m)	Rt (N)	sinkage (m)
Mesh	1,409,101		1,353,145	
CFD (present study)	13.72	0.00664	1.22	0.0012
E(%D)	4.99	0.61	9.91	14.29
EFD	14.44 (Deng et al., 2014)		1.11 (Martić et al., 2019)	0.0014 (Bechthold and Kastens, 2020)
CFD (Toxopeus et al., 2013)		0.0066		

Next, to estimate the grid convergence uncertainty of the CFD solution, we used the grid convergence index (GCI) method, which is based on the Richardson extrapolation. Park et al. (2015), Tezdogan et al. (2016), and Demirel et al. (2017) recently used the GCI method to evaluate the numerical uncertainty in computational results. The verification process with the GCI method was followed according to the method described by Celik et al. (2008).

The numerical convergence ratio R is calculated as follows:

$$R = \frac{\epsilon_{21}}{\epsilon_{32}} \tag{4}$$

Here, it is obtained by $\epsilon_{21} = \phi_2 - \phi_1$ and $\epsilon_{32} = \phi_3 - \phi_2$, which represent the difference in the solution values between medium-fine and coarse-medium, respectively. ϕ_1, ϕ_2, and ϕ_3 represent the solutions calculated for fine, medium, or coarse mesh.

The apparent order p of the method can be obtained as follows:

$$p = \frac{\ln(\epsilon_{32}/\epsilon_{21})}{\ln(r_{32})} \tag{5}$$

Here r_{32} is the grid refinement factor calculated by $r_{32}=h_{coarse}/h_{medium}$ ($\sqrt{2}$ in this study).

The extrapolated values are calculated as shown in Equation (6):

$$\phi_{ext}^{32} = \frac{r_{32}^p \phi_2 - \phi_3}{r_{32}^p - 1} \tag{6}$$

The approximate and extrapolated relative errors are obtained by the following equations, respectively:

$$e_a^{32} = \left| \frac{\phi_2 - \phi_3}{\phi_2} \right| \tag{7}$$

$$e_{ext}^{32} = \left| \frac{\phi_{ext}^{32} - \phi_2}{\phi_{ext}^{32}} \right| \tag{8}$$

The medium-grid convergence index is calculated as follows:

$$GCI_{med}^{32} = \frac{1.25 e_a^{32}}{r_{32}^p - 1} \tag{9}$$

The number of cells used for calculating the grid convergence for the actual size of KVLCC2 is shown in Table 4. The grid convergence study using the GCI method shows that the numerical uncertainty of the sinkage and resistance are estimated to be 1.04% and 4.76%, respectively, based on the medium mesh (Table 5). *Ct* denotes the nondimensionalized resistance by ($0.5\rho S V_s^2$). Verification for the time step convergence study was performed while gradually decreasing the time step from $0.0045L/V_S$, and the results are shown in Table 6.

Table 4. Cell numbers for each mesh configuration

Mesh configuration	Total number of cells
Coarse	724,531
Medium	1,331,705
Fine	2,652,522

Table 5. Grid convergence study for sinkage and resistance of KVLCC2 at *H/T*=1.2

	sinkage/L	*Ct*
ϕ_1	-0.000821	0.002435
ϕ_2	-0.000827	0.002375
ϕ_3	-0.000873	0.002197
R	0.1304	0.3371
p	5.8772	3.1377
ϕ_{ext}^{32}	-0.000820	0.002466
e_a^{32}	5.56%	7.49%
e_{ext}^{32}	0.84%	3.67%
GCI_{med}^{32}	1.04%	4.76%

Table 6. Time step convergence study for sinkage and resistance of KVLCC2 at *H/T*=1.2

	sinkage/L	*Ct*
ϕ_1	-0.000827	0.002375
ϕ_2	-0.000826	0.002380
ϕ_3	-0.000824	0.002432
R	0.32	0.0959
p	3.2877	6.7642
ϕ_{ext}^{32}	-0.000828	0.002375
e_a^{32}	0.10%	2.19%
e_{ext}^{32}	0.05%	0.23%
GCI_{med}^{32}	0.06%	0.29%

As the verification confirmed, performing numerical calculations using a medium mesh appears to be efficient. Therefore, when simulating the actual vessel size in this study, the calculations were performed by selecting the medium mesh size as the base.

3.2 Analysis of longitudinal squat

Fig. 4 shows the trim angle and sinkage when DTC and KVLCC2 move in a straight forward direction. Trim and sinkage tended to differ slightly depending on the depth. Trim by head is a positive value, whereas trim by stern is a negative value. DTC is trim by stern, and KVLCC2 is trim by head. If C_B is greater than 0.7 it becomes trim by head, and if it is less than 0.7 it becomes trim by stern (Barrass and Derrett, 2006). This simulation results show the same tendency. The amount of trim change of DTC is much smaller than that of KVLCC2. The influence of water depth also seems to be relatively less. However, KVLCC2 is more affected by water depth than DTC.

Regarding the sinkage change, the sinkage of both ships gradually increases as the water depth becomes shallower. The amount of change of DTC is greater than that of KVLCC2, and changes with the water depth.

Fig. 5 shows the result of calculating the increase in draft, that is, the longitudinal squat based on the trim angle and sinkage that occur when the ship advances. These values are dimensionless with each length of ship. KVLCC2 is represented as a relatively small value, because the sinkage is smaller than that of the DTC. However, for DTC, the longitudinal squat value becomes larger as the water depth becomes shallower, due more to the larger sinkage change than the trim change.

The UKC reduction ratio given in Fig. 6 was obtained from the following equation (increasing this value means that the squat value is larger and UKC decreases more):

$$UKC\ reduction\ ratio = 1 - \frac{DUKC}{SUKC} \tag{10}$$

Because KVLCC2 has a small longitudinal squat value, the change in UKC is also relatively small, showing a reduction ratio of approximately 8% at *H/T*=1.2. For DTC at *H/T*=2.0 and 1.5, the reduction ratios are approximately 11% and 24%, respectively. However, at *H/T*=1.2, the ratio increases rapidly, to approximately 65%. DTC appears to be larger than KVLCC2 in terms of the decrease in the overall clearance depth, because of the shallow water. Both ships are considered to need more attention in very shallow water.

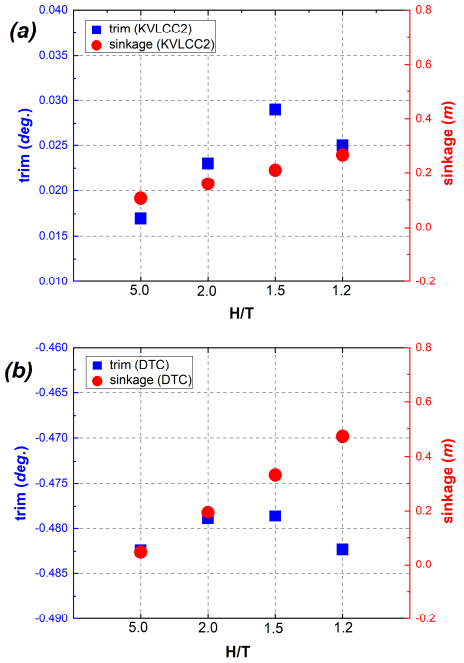

Fig. 4. Comparison of sinkage and trim according to the ratio of water depth to draft: (a) KVLCC2; (b) DTC.

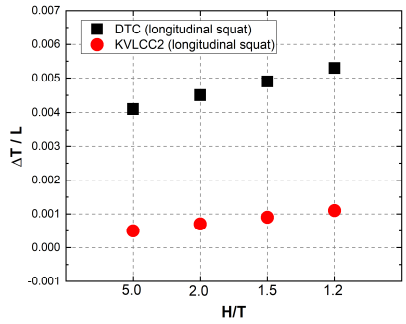

Fig. 5. Comparison of dimensionless longitudinal squat for KVLCC2 and DTC according to the ratio of water depth to draft.

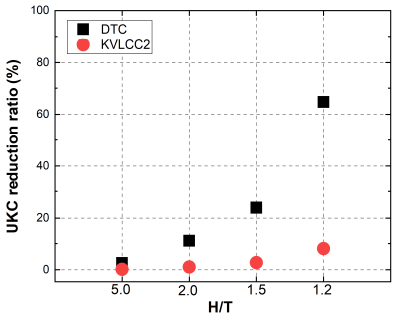

Fig. 6. UKC reduction ratio for KVLCC2 and DTC due to the longitudinal squat.

Figs. 7 and 8 show the free surface and pressure distribution on the bottom of the ship. Subtracting the hydrostatic pressure component expresses the pressure distribution. Fig. 7 shows the simulation results for KVLCC2. At *H/T*=5.0, the pressure at the middle of the ship's bottom is slightly higher than at other parts. The pressure at the stern end is estimated to be higher than at the fore end, which causes the vessel to be trim by head. For *H/T*=2.0, the high-pressure distribution at the middle of the ship's bottom disappears. As the water depth becomes shallower with *H/T*=1.5, the pressure at the fore and aft bottom is lower than that at the center. The pressure on the fore part seems to decrease more widely than on the stern. At *H/T*=1.2, which is the shallowest depth, the low-pressure distribution at the fore and stern bottom expands to the middle of the hull. The pressure at the bottom of the bow is lower than that of the aft. Although the change in water surface is not very evident, the small amount of free surface descent is observed in the bow part as the water depth becomes shallower.

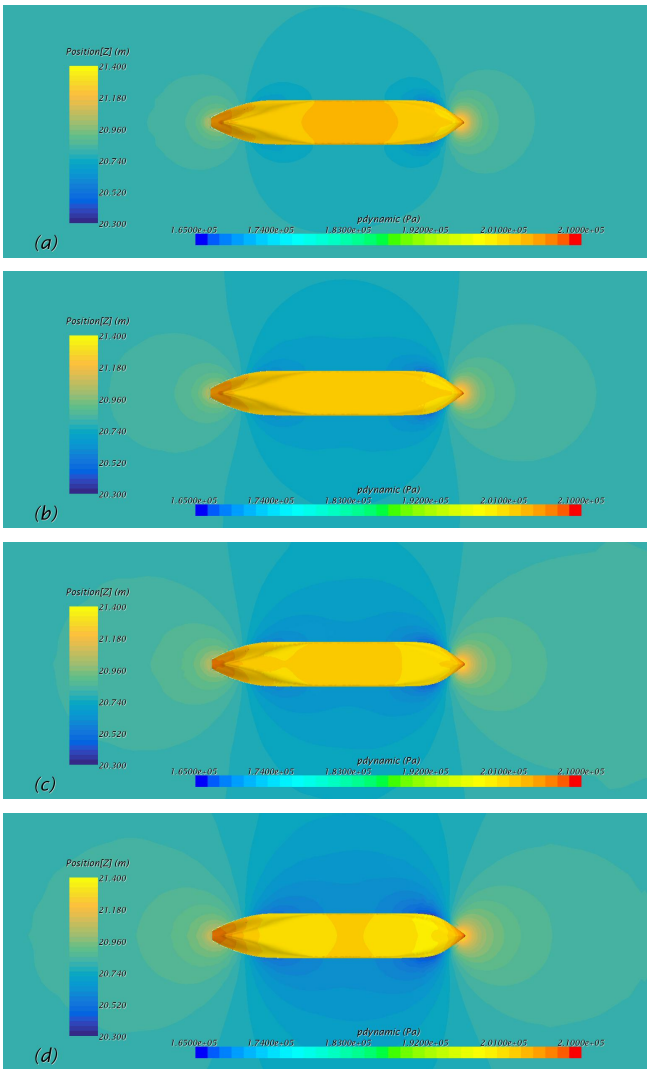

Fig. 7. Free surface and pressure distribution on KVLCC2 upon advancing: (a) *H/T*=5.0; (b) *H/T*=2.0; © *H/T*=1.5; (d) *H/T*=1.2.

Fig. 8 shows the simulation results for DTC. At *H/T*=5.0, a high pressure is observed at the fore and stern. At *H/T*=2.0, the pressure acting on the fore and stern appears to be slightly smaller. At *H/T*=1.5, the pressure decreases throughout the central part of the ship. At *H/T*=1.2, the pressure distribution on the rear side in the stern direction from the midship lowers. The free surface gradually decreases around the hull as the water depth becomes shallower. In particular at *H/T*=1.2, when the water depth is the shallowest, the surface also clearly descends in the lower part of the pressure on the bottom, just behind the center of the ship.

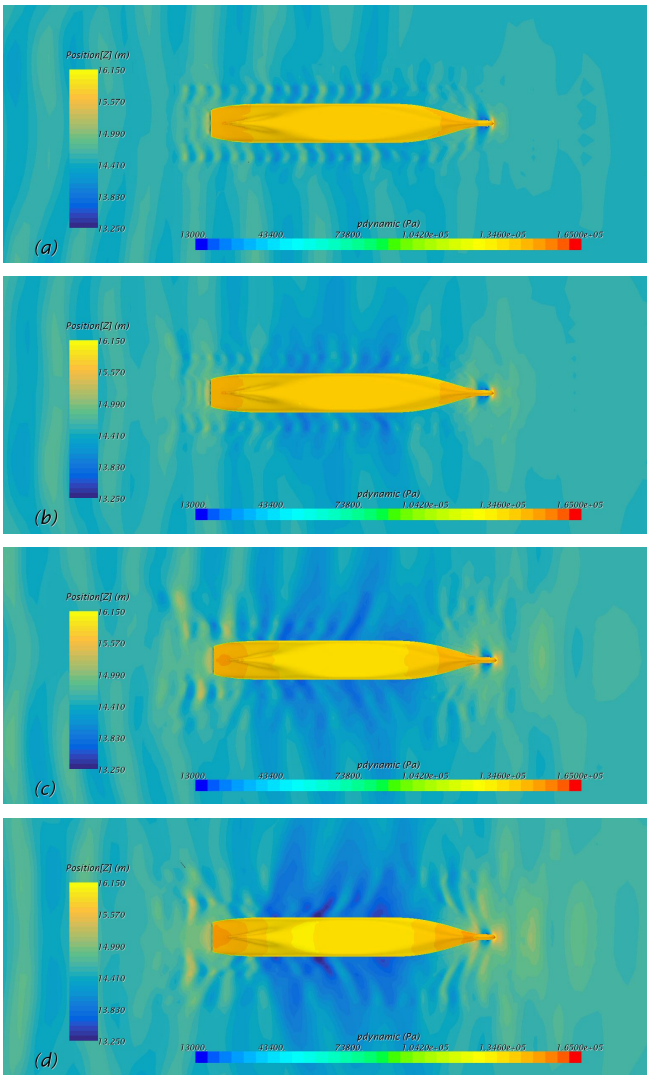

Fig. 8. Free surface and pressure distribution on DTC upon advancing: (a) *H/T*=5.0; (b) *H/T*=2.0; © *H/T*=1.5; (d) *H/T*=1.2.

3.3 Analysis of lateral squat

This section explains how the contents can be used to estimate the amount of UKC reduction by obtaining the heel angle generated in the turning vessel.

It can be observed from Fig. 9 that when a ship turns at speed V_S in a stationary state, it lists due to a roll moment and the draft increases. The figure and the draft calculation process follows the textbook by Barrass and Derrett (2006). The new draft, which is due to the list, can be obtained using the following equation:

$$New\ draft,\ XY = \frac{1}{2}B \times \sin\theta + AC \times \cos\theta \qquad (11)$$

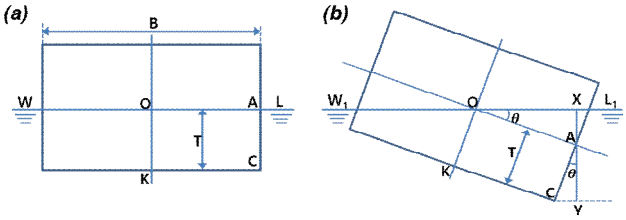

Fig. 9. Increase of draft due to heel in turning, referred from Barrass and Derrett (2006): (a) upright vessel; (b) listed vessel with a heel angle θ.

The turning direction is toward the port side. Because of the absence of a rudder in the bare hull state, the force acting on the rudder was not considered. The port-side direction of the turning vessel is indicated as the inward side, and the starboard side, which is the direction to the opposite of turning, is indicated as the outward side.

The heel angle, which is the largest during turning, is calculated in a steady state rather than an accelerated one. The inward heel angle is negative, whereas the outward heel angle is positive.

Fig. 10 shows the change characteristics of the heel angle for the DTC and KVLCC2. The absolute value of the heel angle shows that the DTC container ship is much larger than the KVLCC2 tanker ship. This trend corresponds to the results of research by Verwilligen et al. (2019), finding that the effect of dynamic heel due to wind, turning, etc., is more extremely limited in bulk carriers (full-form ships) than container ships (fine-form ships).

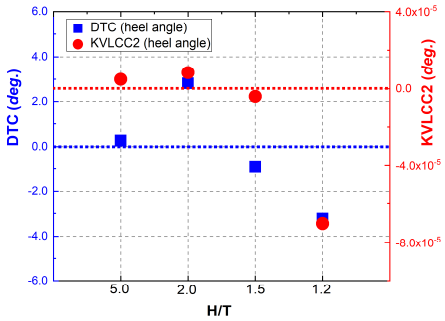

Fig. 10. Comparison of heel angle for KVLCC2 and DTC according to the ratio of water depth to draft.

Both types of ships show outward heel angles up to *H/T*=5.0 and 2.0. However, when the water depth becomes shallow, such as at *H/T*=1.5 and 1.2, an inward heel is generated by the shallow water effect. The inward heel increases rapidly, particularly in very

shallow water, such as at *H/T*=1.2. A detailed cause analysis is discussed in Figs. 13-16, which show the CFD simulation results.

Fig. 11 presents the result obtained by using Equation (11) to calculate the increased draft, which is the lateral squat based on the heel angle caused by the turning of the ship. This is a dimensionless value with the breadth of each ship. KVLCC2 has a very small heel angle that is almost zero. However, for DTC, the lateral squat value increases as the water depth becomes shallower. It decreases at *H/T*=1.5, seemingly because the maximum value decreases as the heel angle becomes negative as it changes from the outward to inward heel.

Fig. 12 shows the reduction ratio of the UKC due to lateral squat. For KVLCC2, the maximum value of the heel angle is very small, which indicates that there is almost no change in the UKC. For DTC, the reduction ratio is less than 10% at *H/T*=2.0 and 1.5, but is large, approximately 50%, at *H/T*=1.2. Therefore, it is important to note that when the ship turns in a very shallow area, where the clearance depth is approximately 20% of the draft, the distance between the bottom of the hull and the seabed decreases rapidly due to the inward heel.

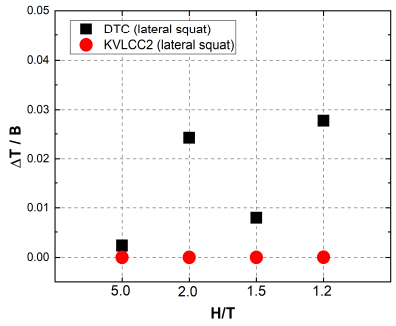

Fig. 11. Comparison of dimensionless lateral squat for KVLCC2 and DTC according to the ratio of water depth to draft.

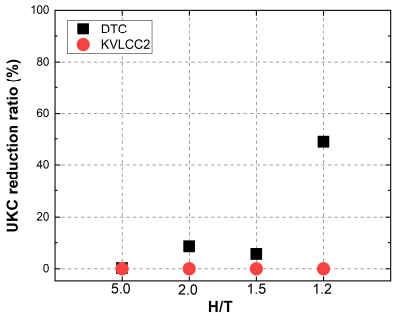

Fig. 12. UKC reduction ratio for KVLCC2 and DTC due to the lateral squat.

Figs. 13 and 14 show the free surface and pressure distribution acting on KVLCC2. *H/T*=2.0 denotes the outward heel state, where the heel's angle value is positive, and *H/T*=1.2 shows the simulation result in the inward state, where the angle value is negative.

In Fig. 13 at *H/T*=2.0, the pressure distribution at the bottom of the ship does not show a significant difference between port and starboard sides. However, the pressure is slightly more active at the fore and stern ends of the inward side than on the outward side. It is assumed that this pressure causes an outward heel of the turning vessel.

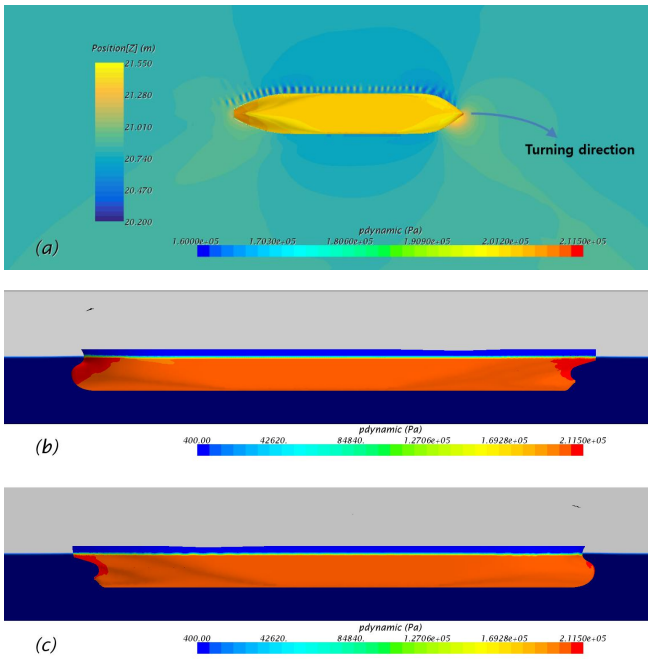

Fig. 13. Free surface and pressure distribution on KVLCC2 upon turning at *H/T*=2.0: (a) bottom view; (b) inward side view; (c) outward side view.

Fig. 14 shows the simulation results for very shallow water with *H/T*=1.2. Observing the pressure distribution on the side, it appears that the pressure at the fore end of the inward side is larger than that at the outward side, however the pressure distribution at the stern end does not show much difference on either side. The pressure at the bottom of the center on the outward side is slightly larger, and the pressure at the bottom of the stern on the inward side is distributed to be lower than its surroundings. This uneven pressure distribution on the bottom of the ship is analyzed to be the cause of the shallow water effect that acts on the turning vessel. It causes the vessel to list inward, which is the turning direction.

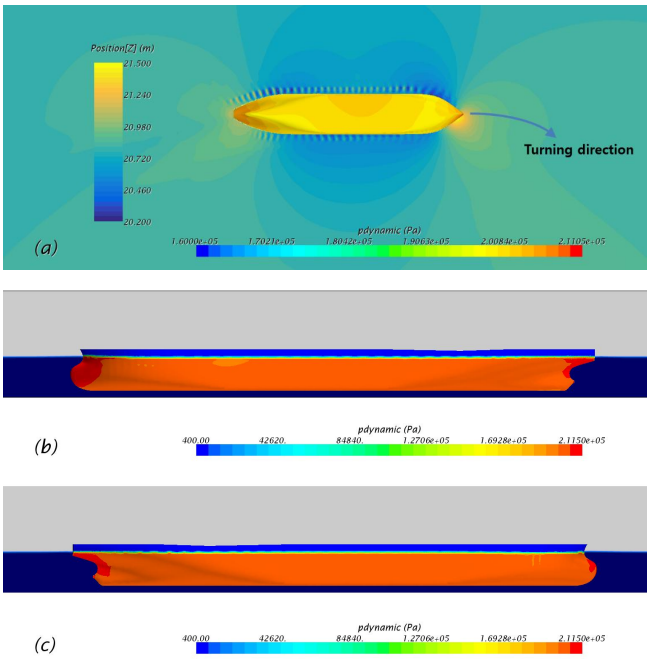

Fig. 14. Free surface and pressure distribution on KVLCC2 upon turning at *H/T*=1.2: (a) bottom view; (b) inward side view; (c) outward side view.

Figs. 15 and 16 show the free surface and pressure distribution acting on the DTC at *H/T*=2.0 and 1.2, respectively. Fig. 15 shows the results at *H/T*=2.0. When observing the pressure distribution on the side, the pressure in the bulbous bow part of the outward side is smaller than that on the inward side. At the stern side, the pressure on the inward side is higher than that on the outward side. For the pressure at the bottom of the ship, its distribution from the stern skeg on the inward side to the stern end seems to be larger than that on the outward side. It is estimated that an outward heel occurs due to the uneven pressure distribution on the ship's side and bottom.

Fig. 16 shows the results for *H/T*=1.2. The pressure at the fore end of the inward side is greater than that on the outward side, and the pressure on the outward side of the stern side appears to be greater than that on the inward side. The central part of the hull side has lower pressure distribution at the inward side. The pressure at the center of the bottom of the outward portion is larger and the pressure from the center of the bottom of the inward to the stern boss direction is distributed lower. This pressure distribution at the bottom of the ship is similar to that for KVLCC2, as shown in Fig. 14, which is the result calculated under similar very shallow water conditions. This shallow water effect causes the pressure at the bottom of the stern on the turning side to decrease. The pressure in the center of the bottom of the opposite side of turning increases, which generates an inward heel.

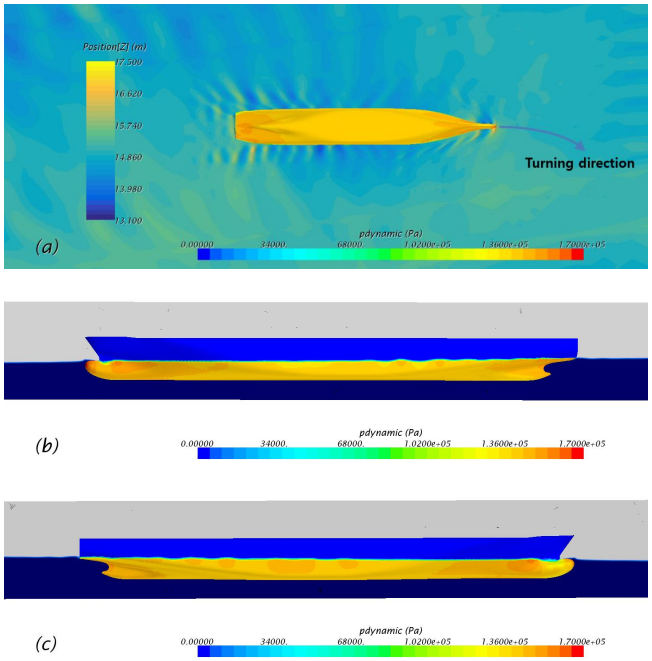

Fig. 15. Free surface and pressure distribution on DTC upon turning at *H/T*=2.0: (a) bottom view; (b) inward side view; (c) outward side view.

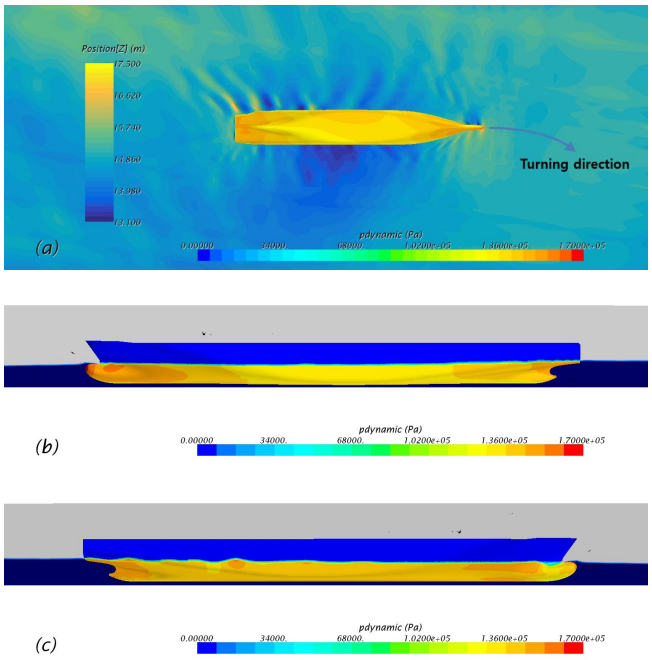

Fig. 16. Free surface and pressure distribution on DTC upon turning at *H/T*=1.2: (a) bottom view; (b) inward side view; (c) outward side view.

Figs. 17 and 18 show the pressure distribution of KVLCC2 and DTC at *H/T*=1.2 and 2.0 as a transversal plane. KVLCC2 has a relatively small change in water surface, and it is estimated that the inclination of the hull is not noticeable. On the other hand, the inclination of the hull to the inward or outward side is relatively large in DTC.

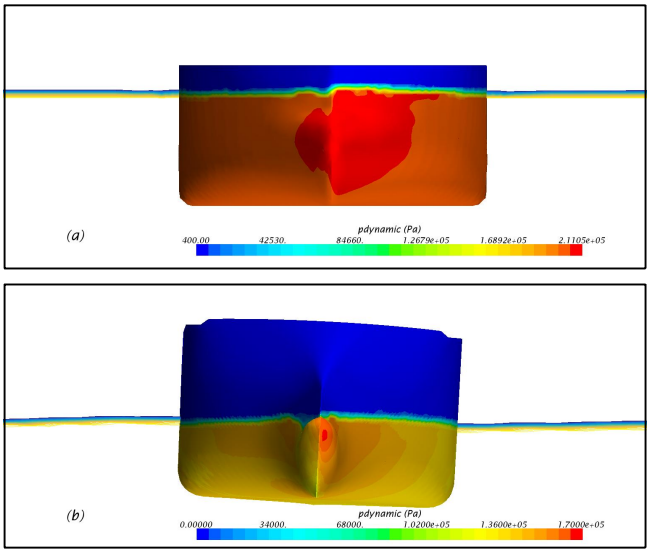

Fig. 17. Transversal plane view of pressure distribution upon turning at *H/T*=1.2: (a) KVLCC2; (b) DTC.

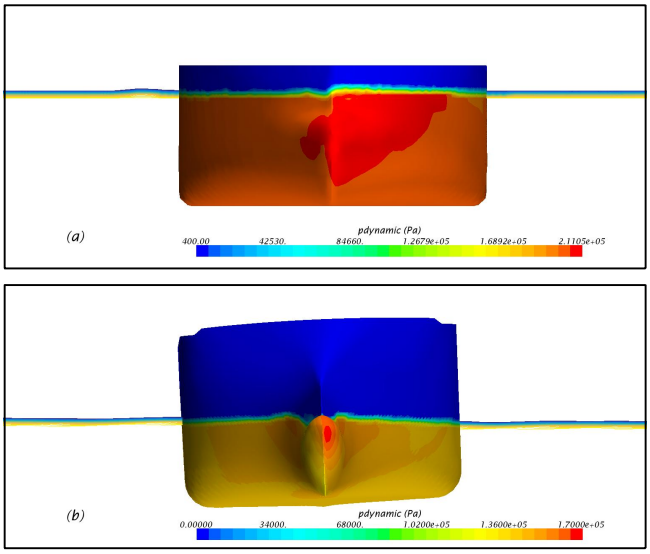

Fig. 18. Transversal plane view of pressure distribution upon turning at *H/T*=2.0: (a) KVLCC2; (b) DTC.

4. Conclusions

In this CFD-based study, the longitudinal squat was calculated by considering the amount of change in the trim angle and sinkage due to the advancing ship's vertical movement. The heel angle caused by the roll moment acting on the turning vessel was obtained, and lateral squat was calculated based on this list effect, to analyze the reduced UKC.

The trim change in DTC was much smaller than that in KVLCC2. Regarding the sinkage change, the sinkage of both ships increased gradually as the water depth became shallower. The amount of sinkage change in DTC was greater than that in KVLCC2. As KVLCC2 had a small longitudinal squat value, the change in UKC was also relatively small. It showed a reduction ratio of approximately 8% at *H/T*=1.2 for KVLCC2. In the case of DTC, it increased rapidly to approximately 65%.

The absolute value of the heel angle of the DTC container ship was much larger than the KVLCC2 tanker ship. Both ships showed outward heel angles up to *H/T*=5.0 and 2.0. When the water depth became shallow, such as *H/T*=1.5 and 1.2, an inward heel was generated by the shallow water effect. In very shallow water, *H/T*=1.2, the inward heel increased rapidly. For KVLCC2, there was little change in UKC because the maximum value of the heel angle was very small. For DTC, the reduction ratio was less than 10% at *H/T*=2.0 and 1.5, but it was very large approximately 50% at *H/T*=1.2. DTC appeared to be larger than KVLCC2 in terms of the decreased UKC because of shallow water in advancing and turning.

Most studies have not considered the effect of shallow water on the ship list that occurs with a turning vessel. In this study, a new result was derived: a ship turning in a steady state due to the influence of shallow water can incline inward, which is the turning direction.

Grasping the characteristics of the flow field according to water depth, which is different for each ship type, make it possible to predict changes in the clearance depth due the effect of shallow water. Using the results of this study, operators sailing in shallow waters are expected to be able to prepare active countermeasures against changes in ship movements, thereby contributing to improved safety.

References

[1] Alderf, N., E. Lefrancois, P. Sergent, and P. Debaillon(2011), Dynamic ship response integration for numerical prediction of squat in highly restricted waterways, International Journal for Numerical Methods in Fluids, Vol. 65, pp. 743-763.

[2] Barrass, C. B. and D. R. Derrett(2006), Ship stability for masters and mates, 6th ed.; Butterworth-Heinemann: Oxford, UK, 2006.

[3] Bechthold, J. and M. Kastens(2020), Robustness and quality of squat predictions in extreme shallow water conditions based on RANS-calculations, Ocean Engineering, Vol. 197, 106780.

[4] Celik, I. B., U. Ghia, P. J. Roache, C. J. Freitas, H. Coleman, and P. E. Raad(2008), Procedure for estimation and reporting of uncertainty due to discretization in CFD applications. Journal of Fluids Engineering, Vol. 130, 078001-1–078001-4.

[5] Demirel, Y. K., O. Turan, and A. Incecik(2017), Predicting the effect of biofouling on ship resistance using CFD. Applied Ocean Research, Vol. 62, pp. 100-118.

[6] Deng, G., E. Guilmineau, A. Leroyer, P. Queutey, M. Visonneau, and J. Wackers(2014), Simulation of container ship in shallow water at model scale and full scale. In Proceedings of the Third Chinese National CFD Symposium on Ship and Offshore Engineering, Dalian, China, 25 July 2014.

[7] Ferziger, J. H. and M. Peric(2002), Computational Methods for Fluid Dynamics, 3rd ed.; Springer: Berlin, Germany, 2002.

[8] Gourlay, T.(2008), Slender-body methods for predicting ship squat, Ocean Engineering, Vol. 35, pp. 191-200.

[9] Kijima, K., R. Tanaka, Y. Furukawa, and T. Kaneko(2002), Simple prediction method on squat, Transactions of the West-Japan Society of Naval Architects, No. 103, pp. 101-110.

[10] Lataire, E., M. Vantorre, and G. Delefortrie(2012), A prediction method for squat in restricted and unrestricted rectangular fairway, Ocean Engineering, Vol. 55, pp. 71-80.

[11] Lee, S. M. and C. B. Hong(2017), Study on the course stability of very large vessels in shallow water using CFD, Ocean Engineering, Vol. 145, pp. 395-405.

[12] Martić, I., G. Chillcce, M. Tello Ruiz, J. Ramirez, N. Degiuli, and O. el Moctar(2019), Numerical assessment of added resistance in waves of the DTC container ship in finite water depths. In Proceedings of the 5th MASHCON, Ostend, Belgium, 19-23 May 2019.

[13] Park, S. H., G. H. Oh, S. H. Rhee, B. Y. Koo, and H. S. Lee(2015), Full scale wake prediction of an energy saving device by using computational fluid dynamics. Ocean Engineering Vol. 101, pp. 254-263.

[14] PIANC(1992), Capability of ship manoeuvring simulation models for approach channels and fairways in harbours. Report of working group no. 20 of permanent technical committee Ⅱ. Supplement to PIANC bulletin, 1992, No. 77.

[15] Tang, X., S. Tong, G. Huang, and G. Xu(2020), Numerical investigation of the maneuverability of ships advancing in the non-uniform flow and shallow water areas, Ocean Engineering, Vol. 195, 106679.

[16] Terziev, M., T. Tezdogan, E. Oguz, T. Gourlay, Y. K. Demirel, and A. Incecik(2018), Numerical investigation of the behaviour and performance of ships advancing through restricted shallow waters, Journal of Fluids and Structures, Vol. 76, pp. 185-215.

[17] Tezdogan, T., A. Incecik, and O. Turan(2016), A numerical investigation of the squat and resistance of ships advancing through a canal using CFD, Journal of Marine Science and Technology, Vol. 21, pp. 86-101.

[18] Toxopeus, S. L., C. D. Simonsen, E. Guilmineau, M. Visonneau, T. Xing, and F. Stern(2013), Investigation of water depth and basin wall effects on KVLCC2 in manoeuvring motion using viscous-flow calculations, Journal of Marine Science and Technology, Vol. 18, pp. 471-496.

[19] Verwilligen, J., K. Eloot, M. Mansuy, and M. Vantorre(2019), Full-scale measurements of vertical motions on ultra large container vessels in Scheldt estuary, Ocean Engineering, Vol. 188, 106264.

[20] Xu, H., M. A. Hinostroza, Z. Wang, and C. Guedes Soares(2020), Experimental investigation of shallow water effect on vessel steering model using system identification method, Ocean Engineering, Vol. 199, 106940.

[21] Yuan, S., L. Xia, Z. J. Zou, and L. Zou(2019), CFD-based numerical prediction of vertical motions and resistance for DTC container carrier in shallow water waves. In Proceedings of the 5th MASHCON, Ostend, Belgium, 19-23 May 2019.

[22] Yun, K. H., B. J. Park, and D. J. Yeo(2014a), Experimental study of ship squat for KCS in shallow water, Journal of the Society of Naval Architects of Korea, Vol. 51, No. 1, pp. 34-41.

[23] Yun, K. H., K. R. Park, and B. J. Park(2014b), Study of ship squat for KVLCC2 in shallow water, Journal of the Society of

Naval Architects of Korea, Vol. 51, No. 6, pp. 539-547.

[24] Zeng, Q., R. Hekkenberg, and C. Thill(2019), On the viscous resistance of ships sailing in shallow water, Ocean Engineering, 2019, Vol. 190, 106434.

[25] Zeng, Q., R. Hekkenberg, C. Thill, and H. Hopman(2020), Scale effects on the wave-making resistance of ships sailing in shallow water, Ocean Engineering, Vol. 212, 107654.

Received : 2021. 05. 06.
Revised : 2021. 05. 21.
Accepted : 2021. 05. 28.